energies

MDPI

Article

Effects of SiO_2 Nanoparticle Dispersion on the Heat Storage Property of the Solar Salt for Solar Power Applications

Zhao Li [1], Liu Cui [1,*], Baorang Li [1] and Xiaoze Du [2,*]

[1] Key Laboratory of Power Station Energy Transfer Conversion and System, North China Electric Power University, Ministry of Education, Beijing 102206, China; zhaoli@ncepu.edu.cn (Z.L.); libr@ncepu.edu.en (B.L.)
[2] School of Energy and Power Engineering, Lanzhou University of Technology, Lanzhou 730050, China
* Correspondence: liucui@ncepu.edu.cn (L.C.); duxz@ncepu.edu.cn (X.D.)

Abstract: The effects of SiO_2 nanoparticles on the heat storage properties of Solar Salt ($NaNO_3$-KNO_3) are studied using experimental and molecular dynamics (MD) simulations. The experiment results show the specific heat capacity of the molten salt-based nanofluids is higher than that of the pure base salt. We focus on the inference regarding the possible mechanisms behind the enhancement of the specific heat capacity which are considered more acceptable by the majority of researchers, the energy and force in the system are analyzed by MD simulations. The results demonstrate that the higher specific heat capacity of the nanoparticle is not the reason leading to the heat storage enhancement. Additionally, the analysis of potential energy and system configuration shows that the other possible mechanisms (i.e., interfacial thermal resistance theory and compressed layer theory) are only superficial. The forces between the nanoparticle atoms and base salt ions construct the constraint of the base salt ions, further forms the interfacial thermal resistance, and the compressed layer around the nanoparticle. This constraint has a more stable state and requires more energy to deform it, leading to the improvement of the heat storage property of nanofluids. Our findings uncover the mechanisms of specific heat capacity enhancement and guide the preparation of molten salt-based nanofluids.

Keywords: molten salt; nanoparticle; specific heat capacity; mechanisms; energy; force

Citation: Li, Z.; Cui, L.; Li, B.; Du, X. Effects of SiO_2 Nanoparticle Dispersion on the Heat Storage Property of the Solar Salt for Solar Power Applications. *Energies* **2021**, *14*, 703. https://doi.org/10.3390/en14030703

Received: 18 December 2020
Accepted: 26 January 2021
Published: 29 January 2021

1. Introduction

With the exhaustion of fossil fuels and the growth of pollutant emissions caused by burning fossil fuels, it is urgent for us to develop sustainable and environmentally friendly energy sources. The installed capacity of the solar thermal power system has grown rapidly in recent years, since large scale concentrated solar power (CSP) has advantages including mature technology, stable power supply, etc. [1]. In the CSP system, molten salt is an important heat transfer and storage medium, since it has the features of low cost, large reserves, and is environmentally friendly. In addition, the molten salt can remain thermally stable at a relatively high working temperature, which is also necessary and important for the thermodynamic cycle in the CSP system [2–6]. However, the thermophysical properties of molten salt at their working temperature range are disappointing (i.e., the specific heat capacity (SHC) is lower than 2 $J{\cdot}g^{-1}{\cdot}K^{-1}$ and the thermal conductivity (λ) is about 0.3~0.6 $W{\cdot}m^{-1}{\cdot}K^{-1}$) in the liquid phase [7–13]. This is important as these are essential properties for heat transfer fluid (HTF) and thermal energy storage (TES) materials. As for TES materials in CSP, the SHC is the most important property. The lower SHC, on the one hand, may lead to a dramatic increase in scale and cost [14]; while on the other hand, it may cause a larger drop in the temperature of the molten salt when working in a steam generator and consequently reduce the cycle efficiency [15]. To improve the thermal energy storage property of molten salt, some researchers propose the method of adding nanoparticles with ultralow loading into molten salt, and satisfactorily, the anomalous enhancement of SHC is

obtained using this method. Xiong et al. [16] explored the preparation method's (i.e., high-temperature melting method and two-step method) influence on the heat storage property on a binary nitrate-SiO_2 nanofluid. As can be seen, the SHC enhancements are 45.56 and 17.38%, respectively for the sample obtained by the high-temperature melting method and two-step method. Shin and Seo [17] studied the size effect of nanoparticle on SHC of a ternary nitrate ($LiNO_3$-$NaNO_3$-KNO_3). The results demonstrated that the enhancement of SHC was 13~16% with 1% wt. SiO_2 nanoparticles and the size of the nanoparticles may have little effect on the SHC enhancement of this ternary nitrate. In addition, Sang and Liu [18] investigated the SHC of a ternary carbonate (K_2CO_3-Li_2CO_3-Na_2CO_3) with different nanoparticles (i.e., SiO_2, CuO, TiO_2, Al_2O_3). They found that the enhancements of SHC were 78.0~116.8, 50.6~73.9, 31.1~56.5, and 50.6~66.5% by adding 1% wt. SiO_2, CuO, TiO_2, Al_2O_3 nanoparticle in the range of 500~540 °C. Moreover, Luo et al. [19] studied the SHC of molten Solar Salt doped with CuO nanoparticles. From their research, the most optimal loading level of CuO nanoparticles was 0.5% wt., and the enhancement of SHC was 11.48%.

In order to explore the reason that leads to the increment in the SHC enhancement, researchers have proposed various empirical models or deductions to explain the reason for the anomalous enhancement of SHC. Three inferences are used to explain the SHC enhancement of the nanofluid proposed by Shin et al. [20], which are widely recognized by lots of researchers. They considered that the higher SHC of nanoparticles (higher than that of the bulk material), the interfacial resistance between the nanoparticle and the base salt, and the compressed layer around the surface of the nanoparticle, are the three main reasons that lead to the enhancement of SHC by inducing nanoparticles. Although progress has been made in terms of discovering mechanisms to enhance the SHC of nanofluids, investigations using experiments or simulations are scarce. We consider that simulation investigations are more effective in exploring the mechanisms of SHC enhancement, since experiments are limited to applications to investigate the micro-effects of nanoparticles, especially for the high-temperature condition.

Solar Salt is the most conventional molten salt used in CSP power plants. Here, the relationship between the addition of SiO_2 nanoparticles and the SHC of Solar Salt is investigated. Firstly, we measured the change in specific heat capacity with nanoparticle loading and temperature using an experimental method and then we investigated the mechanisms of SHC enhancement by molecular dynamics (MD) simulation methods.

2. Experiment

2.1. Nanocomposite Synthesis

The mixture of sodium nitrate ($NaNO_3$, CAS: 7631-99-4) and potassium nitrate (KNO_3, CAS: 7757-79-1) used in this experiment had a purity of 99.99% and was produced by Aladdin Technology, while the additive was selected as SiO_2 (CAS: 7631-86-9) nanoparticles with a diameter of 30 nm, produced by WanJing Technology.

To obtain the nanocomposite with excellent dispersion, we improved the traditional two-step method by using an ultrasonic probe to replace the ultrasonic bath [21] and to lower the evaporating temperature (the lower temperature can avoid agglomeration [22]). The detailed nanocomposite synthesis procedure is shown in Figure 1. In this experiment, the maximum power and amplitude values of the ultrasonic probe device were 1200 W and 60 μm, respectively, which are more than enough to treat the sample with 300 mL water. However, we found that using 100% power and amplitude lead to a high-temperature phenomenon, which lead to serious agglomeration of nanofluids [22]. Therefore, a 50% amplitude value was set in this experiment and a cooling method was also carried out during the ultrasonic experiments. The beaker with the nanofluid in was placed into a bigger beaker, which was filled with an ice–water mixture. Meanwhile, we monitored the temperature every 30 s. After many attempts to select the amplitude, we found that it was difficult to restrain the temperature rise when the amplitude was higher than 50%, since

the maximum input power of our device (1200 W) was relatively high. We believe that the amplitude selection in this paper is reasonable.

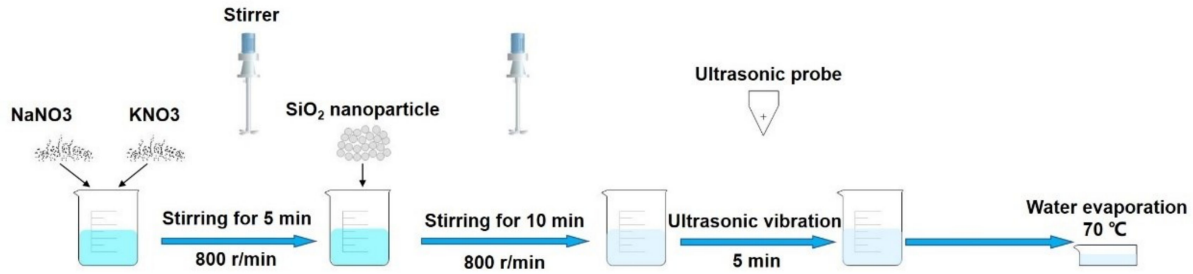

Figure 1. Molten salt-based nanocomposite preparation process.

According to Patricia's research, the optimal nanoparticle concentration (i.e., the largest SHC enhancement that can be obtained at this concentration) is 1 wt% [23]. Hnece, we selected the nanoparticle loading values as 0.2, 0.6, 1.0, and 1.5 wt%, which are either lower or higher than the optimal nanoparticle concentration of 1 wt%. We think this selection of nanoparticle loading values is relatively comprehensive and reasonable. The mass of the sample was selected as 10 g (e.g., 5.94 g of $NaNO_3$, 3.96 g of KNO_3, and 0.1 g SiO_2 nanoparticle for 1.0 wt% sample) and the deionized water was 300 mL.

2.2. Specific Heat Capacity Measurement

The differential scanning calorimeter (DSC, NETZSCH DSC 214) was used to measure the specific heat capacity of the nanofluid. The SHC of the sample can be obtained by three heat flows (i.e., heat flow of pan, pan with sapphire, and pan with sample) and the sapphire SHC in this method.

Based on the TGA measurement result [23], the decomposition temperature of the Solar Salt and Solar Salt-SiO_2 nanofluid were both about 550 °C. Meanwhile, according to the XRD analysis in our previous research [24], we did not find new products in the pure Solar Salt and Solar Salt-SiO_2 nanofluid after exposure to the high-temperature condition (450 °C), which means that no chemical reaction occurred between the SiO_2 nanoparticle and the Solar Salt. Therefore, we set the DSC analyzing temperature range as 130~400 °C, in which the sample can be ensured to remain thermally stable.

The heating rate was 10 °C/min, from room temperature to 130 °C and then this was held for 30 min to ensure that the moisture was removed thoroughly. Heating then continued at a further rate of 10 °C/min to 400 °C, and finally the sample was maintained at 400 °C for 10 min to ensure signal stability. The DSC pan was sealed by a pierced lid, as used in other research studies [25,26], which eliminates possible remaining moisture and maintains the sample in the pan to prevent mass loss. According to our experimental attempt, the pierced lid is appropriate for DSC measurements for molten Solar Salt, since the mass loss can be controlled at about 1~1.5%. More importantly, a relatively lower quantity of salt in the pan is also beneficial to prevent mass loss.

The DSC measurement process was all in the N_2.

2.3. Measurement Uncertainty

The specific heat capacity value can be determined by following Equation (1) [27]:

$$C_{p,s} = C_{p,sapp} \cdot \frac{\Delta q_s \cdot m_{sapp}}{\Delta q_{sapp} \cdot m_s} \quad (1)$$

where C_p, Δq, and m represent the specific heat capacity, the heat flow difference between the specimen and the empty pan, and the mass, respectively. While the subscripts s and sapp denote the sample and sapphire reference material.

The propagation of uncertainty through the mathematical operations can be used to provide the measurement uncertainty in this DSC measurement [28]. Aiming at this measurement, the uncertainty value is dependent on the related parameter deviations, including mass and heat flow, shown in Equation (2) [28].

$$\frac{\delta C_{p,s}}{|C_{p,s}|} = \sqrt{\left(\frac{\delta q_s}{|q_s|}\right)^2 + \left(\frac{\delta q_{sapp}}{|q_{sapp}|}\right)^2 + \left(\frac{\delta m_s}{|m_s|}\right)^2 + \left(\frac{\delta m_{sapp}}{|m_{sapp}|}\right)^2} \quad (2)$$

where δ denotes the deviation of the corresponding value. From the specification of the DSC device and electronic balance used in this experiment, the accuracy of the heat flow and the mass is 0.1 μW and 0.005 mg, respectively. Therefore, the measurement uncertainty is nearly 2%—obtained by Equation (2).

3. Results and Discussions

3.1. Specific Heat Capacity

The specific heat capacity values of the base salt and the nanofluid with a nanoparticle loading of 0.2, 0.6, 1.0, 1.5 wt.% are shown in Figure 2a. As can be seen, the SHC of the pure Solar Salt is about 1.523 J/(g·K), which is consistent with values in the previous literature (i.e., 1.49~1.53 J/(g·K) in the liquid phase) [14,29]. The deviation of less than 5% indicates that our measurement should be reliable. Moreover, the average specific heat capacities of the molten salt-based nanofluids in the liquid phase are 1.536, 1.670, 1.855, and 1.810 J/(g·K), respectively, and the enhancement values of the specific heat capacity are 0.85, 9.65, 21.79, and 18.84% compared with the base salt, respectively. As can be seen, the addition of the nanoparticles can bring an enhancement of the SHC. Additionally, the specific heat of the nanofluids showed different temperature-dependencies even in the liquid phase: increasing specific heat with temperature, uniform ones, and a slightly decreasing one. This was also found in previous research on the molten salt-based nanofluid [4,30–32]. We believe that this results from the change in the nanoparticle dispersion in the measurement process. The nanoparticle dispersion is complex and constantly changing during the DSC measurement process. So, this may cause the C_p to vary irregularly with temperature.

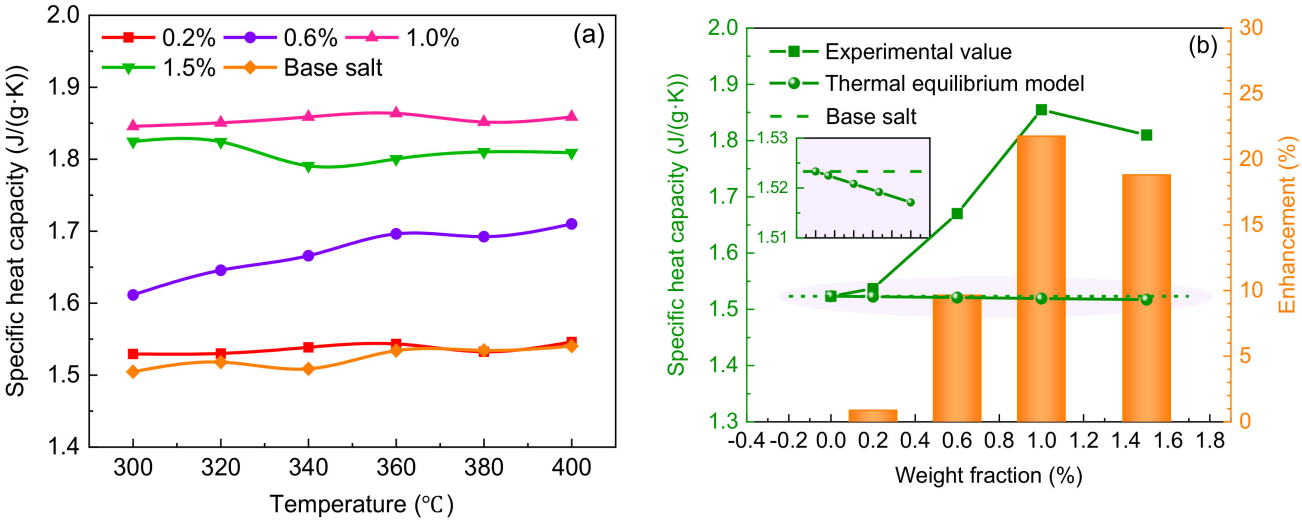

Figure 2. (**a**) Variation in specific heat capacity with temperature for the pure base salt and nanofluids at different nanoparticle loading (0.2, 0.6, 1.0, and 1.5 wt.%). (**b**) Average specific heat capacity (SHC) of nanofluid with nanoparticle loading.

The SHC has a positive correlation with the nanoparticle loading when the nanoparticle loading is lower than 1 wt%. The SHC of the nanofluid with the 1.5 wt% nanoparticle is lower than that of the 1 wt% nanofluid. There may be more aggregates in the nanofluid because of the higher nanoparticle loading, which leads to the SHC decrease in the 1.5 wt% nanofluid compared with the 1 wt% nanofluid.

Usually, the specific heat capacity of the liquid–solid mixture is calculated using the thermal equilibrium model [33], shown in Equation (3), and the specific heat capacity calculated by Equation (3) is shown in Figure 2b. As can be seen, the measured value of the nanofluid specific heat capacity is higher than that of the pure base salt, and it has a positive correlation with the nanoparticle loading. However, the SHC value predicted by the thermal equilibrium model is lower than that of the pure base salt, and it has a negative correlation with the nanoparticle loading. The comparison indicates that the SHC of the nanofluid could not be predicted by the conventional thermal equilibrium model, since it neglects the interaction between the nanoparticle and base salt. It is meaningful and important to investigate the mechanisms of the enhancement of the specific heat capacity, and the correlational research can be found in Section 3.3.

$$C_{\text{mixture}} = \frac{m_{\text{p}}C_{\text{p}} + m_{\text{f}}C_{\text{f}}}{m_{\text{mixture}}} \tag{3}$$

where m and C represent the mass and specific heat capacity, while the subscript p, f, and mixture are the nanoparticle, base salt, and solid and liquid mixture, respectively.

3.2. Material Characterization

The change of the nanofluid thermal properties may be related to the microstructure of the nanocomposite, it is important and meaningful to investigate the micro-structures or nano-structures in the nanofluid system. A scanning electron microscope (SEM), HITACHI SU8010 (HITACHI, Japan) was used in this experiment. The SEM images of the base salt and the nanocomposite with various concentrations of nanoparticles are shown in Figure 3. As can be seen, there are lots of discrete nanoparticles in the nanofluid, and this proves that the SiO_2 nanoparticles were well disperses in the base salt, and the synthesis method and procedure was good. Additionally, there are more aggregates in the nanofluid with 1.5 wt% nanoparticle loading. The nanoparticle loading of 1.5 wt% may be larger than the critical value of the nanoparticle loading mentioned by Ho et al. [30], (i.e., when the loading is larger than the critical value, there will be more aggregation in the system and this may lead to a reduction in the enhancement of the thermophysical properties).

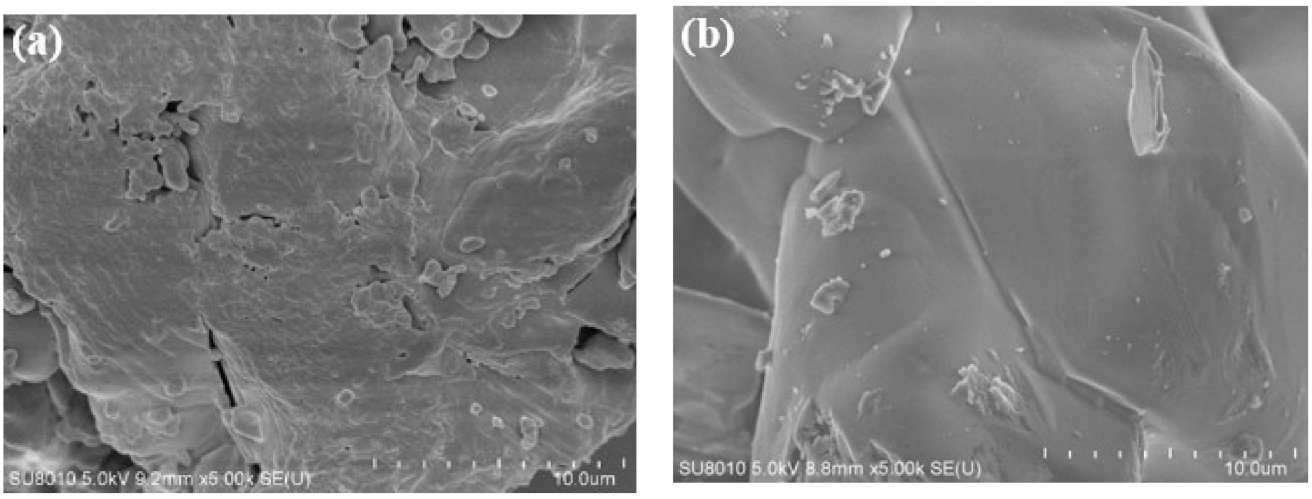

Figure 3. *Cont.*

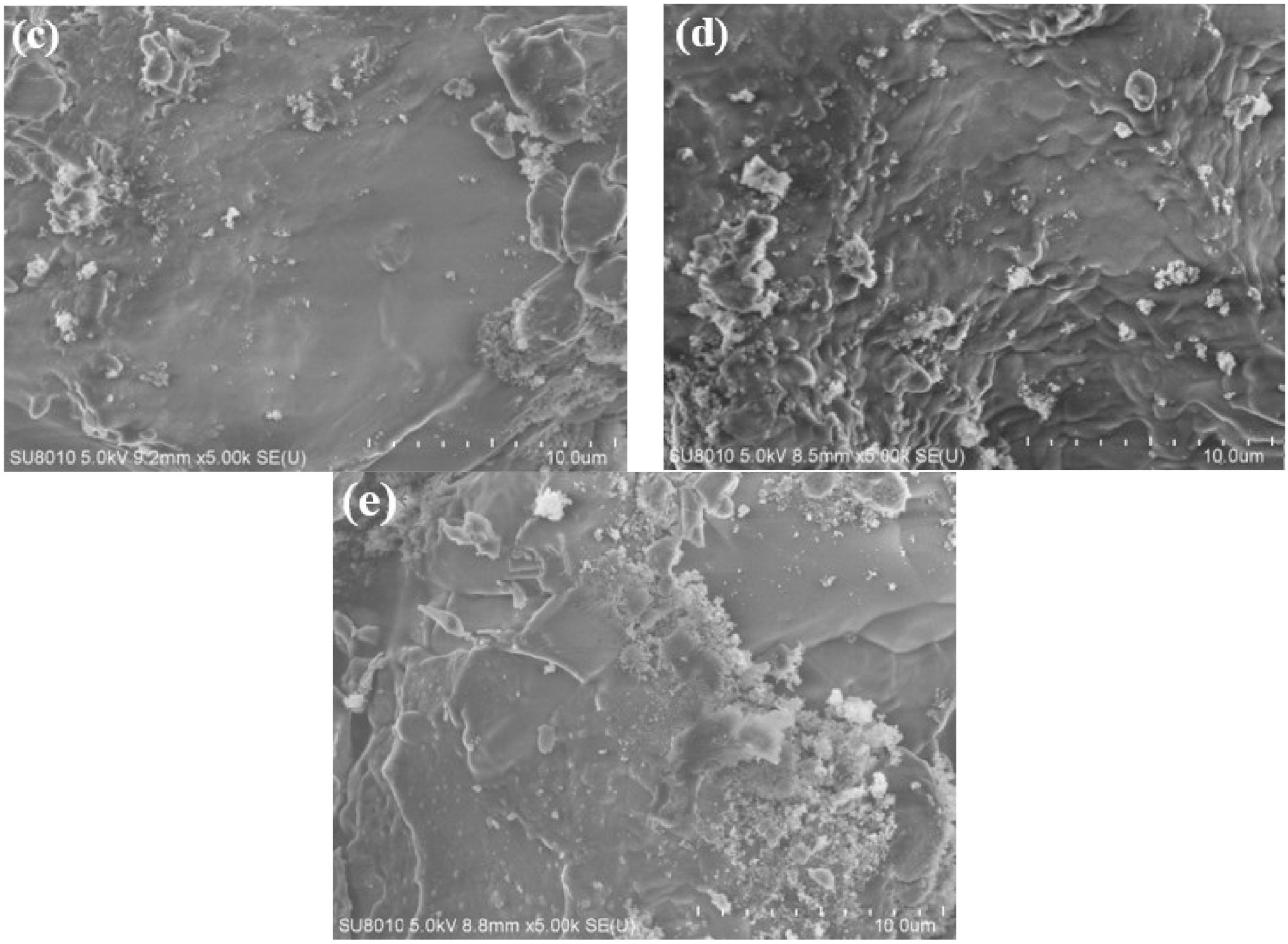

Figure 3. SEM images of the pure base salt and the salt with various loadings: (**a**) pure base salt. (**b**) 0.2 wt%. (**c**) 0.6 wt%. (**d**) 1.0 wt%. (**e**) 1.5 wt%.

3.3. Mechanism Analysis

The nanofluid concept was proposed by Choi et al. [34] in 1995. Based on the collection and analysis of the literatures, there are roughly three mechanisms that are considered more acceptable by the majority of researchers, shown as follows [20]:

(1) Nanoparticles with higher SHCs. The nanoparticle has a higher SHC than that of the corresponding bulk materials. For instance, Wang et al. [35] demonstrated that the SHC of Al_2O_3 is 6~23% higher than that of the Al_2O_3 bulk. Additionally, Zhou et al. [36] also obtained a higher SHC for the CuO nanoparticle by theoretical calculation.

(2) Interfacial thermal resistance. Some researchers believe that there is an interfacial thermal resistance between the nanoparticle and the base salt, which results from the interaction between the nanoparticles and the base salt. Some people compare the interfacial thermal resistance as a kind of virtual spring-mass system [20].

(3) Compressed layer. There is a base salt layer around the nanoparticle with a higher density than that of the base salt far away from the nanoparticle, it is hence named the "compressed layer", and the researchers believe this layer has an enhancement in thermal properties compared to those of the bulk base salt.

However, the experiment could be limited by some factors such as high temperature, corrosion, or the vacuum in the scanning electron microscope (SEM) and transmission electron microscope (TEM), etc. The three mechanisms mentioned above were not investigated deeply and comprehensively until now, and lots of conclusions are made from

deduction and assumption. For this reason, we employed the molecular dynamics (MD) simulation to provide a deeper investigation, since the MD simulation can be used to describe the interaction between the atoms and molecules reliably and it can also obtain the properties and provide a powerful tool to investigate the nanoscale phenomena based on the corresponding potential energy function. The MD simulation research can be found in the following sections.

3.3.1. Details of MD Simulation

In this paper, the Large-scale Atomic/Molecular Massively Parallel Simulator (LAMMPS) [37] was employed to carry out the MD simulation. The process to build the model of the molten salt-based nanofluid can be found in our previous research [38]. The geometric configuration is shown in Figure 4.

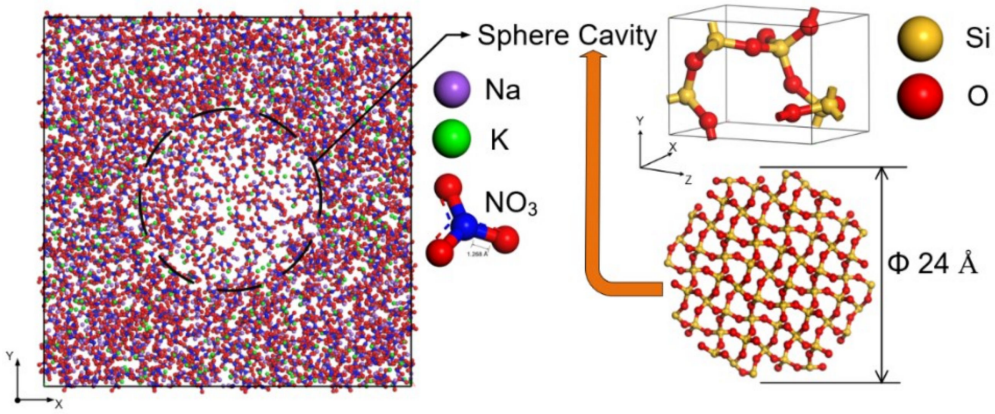

Figure 4. Model of the molten salt nanofluid system.

In the MD simulation of this paper, the time step was set as 0.5 fs and the periodical boundary conditions were applied in the three-dimensional simulation box. The nanofluid system is firstly equilibrated for 6 ns under the NPT ensemble (the Nose-Hoover thermostat and barostat [39,40] were used to fix the system at 1 atm and 573 K higher than the melting point of this binary nitrate). Following this, the nanofluid system was switched into the NVT ensemble and equilibrated for 2 ns. After the equilibration progress, the temperature and total energy were all convergent and the relative error on the total energy of the system $\Delta E/E$ was always in the order of 10^{-5}~10^{-4}. The data production runs were finally performed in the NVT ensemble for another 0.5 ns.

3.3.2. Effects of Nanoparticle SHC

Focusing on the research object in this paper, we calculated the SHC of SiO_2 nanoparticle with a diameter of 10 Å to 50 Å at 573 K shown in Figure 5a. As can be seen, the SHC of the SiO_2 nanoparticle with different diameters is much higher than that of the SiO_2 bulk materials measured by Jund (the SHC of the SiO_2 bulk material was about 1.05 $J \cdot g^{-1} \cdot K^{-1}$ at 573 K [41]). As we all know, the atom can be classified as the inner atom and surface atom. The surface atoms in the lattice of the nanoparticle are less constrained due to the lower number of bonds (relatively lower coordination number)—which leads to the little or uniform force on the surface atom—hence, the surface atom has a low vibration frequency and high vibration amplitude, shown in Figure 5b, which results in a higher surface energy and higher specific heat capacity [20].

Furthermore, it can be revealed that the SHC of the nanoparticle decreases as the nanoparticle size increases, which is attributed to the reduction in the surface atom proportion in the nanoparticle (the surface atom proportion decreases with the nanoparticle diameter, shown in Figure 5b [42]). Based on our simulation results, the SHC of the SiO_2

nanoparticle using in the experiment is lower than 1.29 $J \cdot g^{-1} \cdot K^{-1}$ since the diameter is much large than 5 nm.

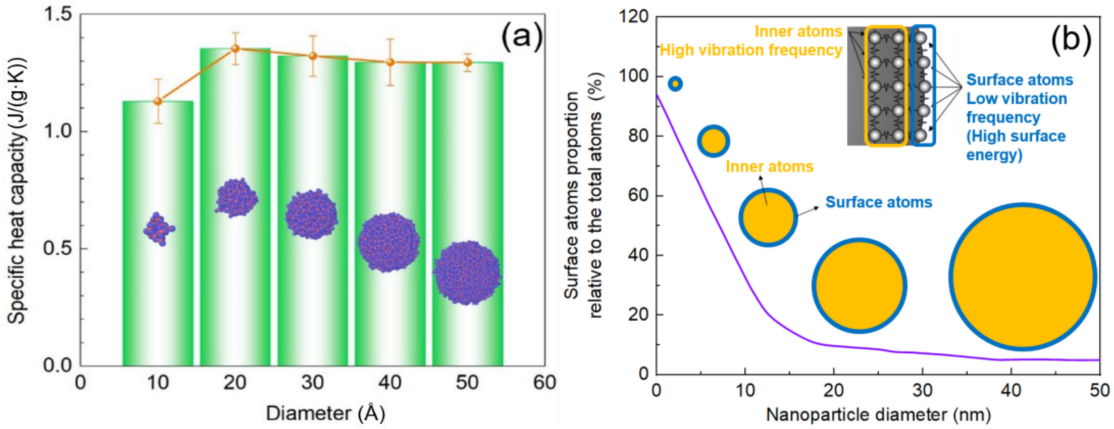

Figure 5. (**a**) Variation in specific heat capacity of SiO_2 nanoparticle with the nanoparticle size. (**b**) Schematic diagram of the size effect on the surface atom proportion and specific heat capacity.

Although the SHC of SiO_2 nanoparticle is much higher than that of the bulk SiO_2, it is still lower than the SHC of the Solar Salt, and the higher SHC of the nanoparticle is probably not responsible for the SHC increment of molten salt-based nanofluid.

3.3.3. Effects of Interaction between Nanoparticle and Base Salt

Based on the previous literature, the interfacial thermal resistance is induced by the interactions between the nanoparticles and the liquid molecules [20]. These interactions may lead to changes in the system energy. Furthermore, the SHC is a thermophysical property that measures how much energy can be stored in a certain amount of the energy of a substance at a certain temperature. We hence, decided to analyze the energy in the nanofluid system—a similar method was also used in Qiao's [43] and Hu's [25] investigations.

In their research, the energy per atom consists of kinetic energy (E_{ke}) and potential energy (E_{pe}) parts, and further, the potential energy can be divided into Van der Waals potential energy (E_{vdwl}), coulombic potential energy (E_{coul}), and molecular potential energy (E_{mol}) (the molecular potential energy is consists of intramolecular bond (E_{bond}), angle (E_{angle}), and improper (E_{impro}) potential energy, respectively), giving the energy as

$$\begin{aligned} E_{total} &= E_{ke} + E_{pe} \\ &= E_{ke} + E_{vdwl} + E_{coul} + E_{mol} \\ &= E_{ke} + E_{vdwl} + E_{coul} + E_{bond} + E_{angle} + E_{impro} \end{aligned} \quad (4)$$

However, we found that there is a contradiction between these two investigations. That is, the potential energy decreases with the nanoparticle loading in Qiao's research, and it leads to the enhancement of the specific heat capacity. On the contrary, the potential energy (E_{pe}) has a positive correlation with the nanoparticle loading in Hu's result. The authors believed that the increment of the potential energy means there is a stronger energy storage ability for the system. Obviously, the results are contradictory. We are hence inclined to explore the reason leading to the contradiction. Inspired by the concept of the thermal equilibrium model and the weighted average method, we conjecture that the relative magnitude of the potential energy of nanoparticle and base salt may have an impact on the change of the system potential energy. Therefore, we calculated the potential energy of nanoparticle and base salt used in these two investigations, our results are shown in Table 1. As can be seen, the E_{pe} of SiO_2 nanoparticle is significantly lower than that of base salt ($NaNO_3$) at 700 K. This may lead to a decrease in E_{pe} with the

increment of nanoparticle loading. Meanwhile, Table 2 also demonstrates that the E_{pe} of Al_2O_3 nanoparticle is significantly higher than that of base salt at 650 K, leading to the E_{pe} increment of the Al_2O_3 nanofluid system investigated in Hu's research. The same phenomenon can also be found for the other components of energy. Therefore, we can deduce that the energy change is related to the relative magnitude of the corresponding components energy of the nanoparticle and base salt, and the change of the E_{pe} may not be the mechanism of the SHC enhancement.

Table 1. The E_{pe} per atom of nanoparticle and base salt system obtained from Ref. [43] and Ref. [25].

Object	SiO_2 Nanoparticle	$NaNO_3$	Al_2O_3 Nanoparticle	Solar Salt
E_{pe} (J)	−2.133E-18	−2.190E-19	5.735E-18	−2.646E-19

Table 2. The different components of the system energy for nanoparticle and base salt (NP and BS denote nanoparticle and base salt, respectively, and the unit in this table is J).

Substance \ Energy (J)	E_{pe}	E_{ke}	E_{coul}	E_{vdwl}	E_{bond}	E_{angle}
NP	−2.134E-18	1.186E-20	−1.870E-18	−2.636E-19	-	-
BS	−2.195E-19	1.187E-20	−2.430E-19	1.746E-20	3.477E-21	6.560E-21

That is to say, the method to investigate the E_{pe} and establish the relationship between the E_{pe} and SHC in these two pieces of literature is not effective. Meanwhile, these results also cannot reflect the energy variation induced by the interaction between nanofluid and base salt, since it may be uncovered up by the influence of the relative magnitude of the energy, especially for the reason that there is a larger difference in energy between the nanoparticle and base salt.

We must propose an innovative method to characterize the interaction. Similarly, we calculated the different components of the system energy per atom and per interaction, averaged by atom number and interaction number, inspired by the concept of the thermal equilibrium model and weighted average calculation. The calculation formula is shown in Equation (5). The energy value obtained by Equation (5) is defined as $E_{ave,}$* (where * represents the different components of energy—* can be set as pe, vdwl, coul, etc., as mentioned above).

$$E_{nf} = \frac{N_{np} \times E_{np} + N_{bf} \times E_{bf}}{N_{np} + N_{bf}} \quad (5)$$

where E and N represent the energy (the related energy components of the base salt and nanofluid can be found in Table 2) and atom number or interaction number (i.e., bond number, angle number, and improper angle number), while the subscript nf, bf, np represent the nanofluid, base salt, and nanoparticle, respectively.

The energy values obtained by Equation (5) can skillfully eliminate the effect of interactions between the nanoparticle and the base salt, since it only reflects the influence of the relative magnitudes of nanoparticle and base salt energy via averaging the energy by atom number and interaction number directly. Making the comparison between the MD simulation value ($E_{MD,}$*) and the $E_{ave,}$*may help us determine the interaction between the nanoparticle and the base salt. In this paper, we defined the difference value of each component energy (ΔE*) as $\Delta E^* = E_{ave,}$ *-$E_{MD,}$ *. The change of ΔE* with nanoparticle loading for the nanofluid is shown in Figure 6. Figure 6 shows that the ΔE_{ke} is nearly two or three orders of magnitude less than ΔE_{pe}. Hence, we believe that the ΔE_{ke} should not have a significant effect on the system energy. It also agrees well with the theory that the kinetic energy is only related to the system temperature. Therefore, we should pay more attention to the potential energy.

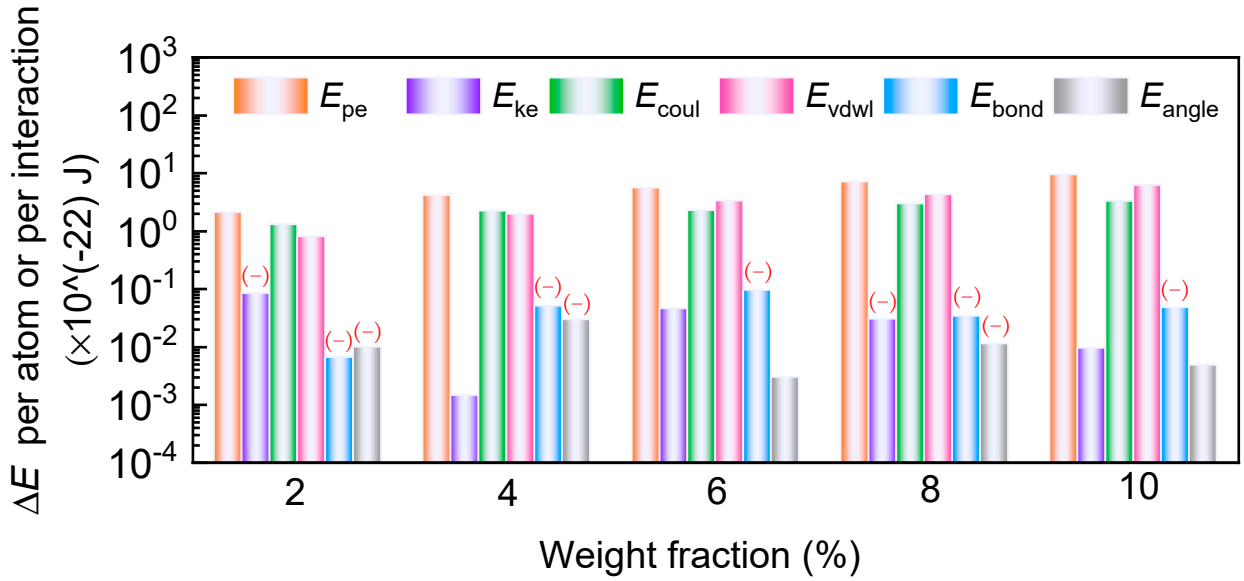

Figure 6. ΔE of the nanofluid system. The (-) in this figure only represents that the corresponding value was originally a negative value, since the logarithmic coordinates do not include negative values).

The ΔE_{pe} for the nanofluid is a positive value, which means $E_{ave,\,pe}$ is larger than $E_{MD,\,pe}$. As can be seen, the interaction between the nanoparticle and base salt leads to a decrease in E_{pe}. In other words, the interaction may construct a potential well in the system. The system should need more energy to overcome this potential well and obtain the targeted state. This potential well plays a role of the extra heat storage. To explore the E_{pe} decrease deeply and in detail, we further investigated the difference value (ΔE) of each component that compose the potential energy, shown in Figure 6. As can be seen, the $\Delta E_{bond,}$ and ΔE_{angle} are both much less than ΔE_{vdwl} and ΔE_{coul}. Hence, the system configuration and the SHC enhancement should not be related to these components of energy. It also demonstrated that the configuration of the NO_3^- ions has nearly no change in the nanofluid system.

Based on this, the ΔE_{vdwl} and ΔE_{coul} should be the major research object in this section. That is to say, the Van der Waals force and Coulomb force dominate the force field in the system. For the nanofluid system, the value of ΔE_{vdwl} and ΔE_{coul} are all positive at each nanoparticle loading. It demonstrates that the Van der Waals force and Coulomb force between the nanoparticle and base salt, further leads to the decrease in the E_{pe}. These two forces may be an attractive force or repulsive force, but they all change the local configuration near the nanoparticle invariably and construct the constraints for the ions of base salt around the nanoparticle, and this constraint acts as an additional thermal storage device.

It is necessary for us to further investigate the ion distribution near the nanoparticle and verify the conclusion about the local configuration variation. The results are shown in Figure 7. It can be seen that there is a peak of density at the distance of 3 Å from the wall of the nanoparticle. In addition, the thickness of the layer with a higher density is about 5 Å, which is similar to previous reports [38,44]. This layer is considered as the compressed layer. For the SiO_2 nanofluid, there are more Na^+ and K^+ and NO_3^- in the compressed layer than there is far away from the nanoparticle. The existence of the compressed layer can verify the deduction that the introduction of the nanoparticle induces the extra force and changes the local configuration of the base salt. In essence, the change in the local configuration of the base salt can be regarded as a kind of constraint from the nanoparticle, and it requires more energy input to deform this constraint.

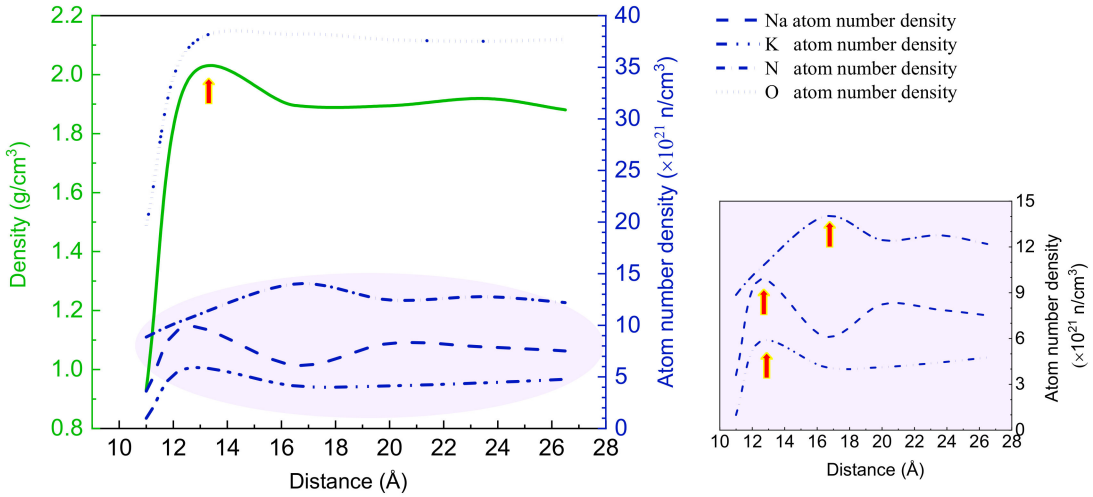

Figure 7. Distribution of atoms in the base salt system (distance represents the distance from the geometric center of the nanoparticle and the atom number density means the atom per cubic centimeter).

To summarize, the introduction of the nanoparticle introduces extra force in the system and further leads to the formation of a compressed layer near the wall of the nanoparticle. There is more constraint on the ions in this layer than there is in the pure base salt due to the attraction or repulsion of the nanoparticle. That is to say, the ions in the compressed layer cannot make free movements unless absorbed energy can overcome the constraint of the nanoparticle when the system is heated, which demanded extra energy. In other words, this appears as a virtual spring system between the nanoparticle and base salt, as the schematic diagram shows in Figure 8. This situation is similar to that happening in the solid–liquid phase change progress. As we all know, the phase change progress can store more energy, which causes the enhancement of specific heat capacity.

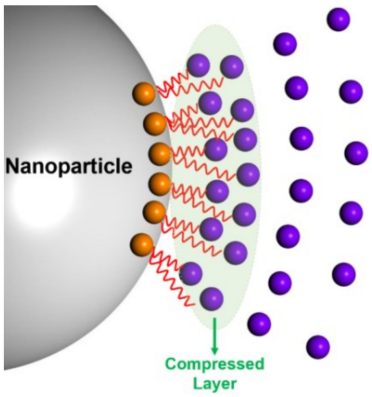

Figure 8. The ions distribution and structure near a nanoparticle.

Furthermore, it is also much clearer as to why the particle in the nanoscale can cause the enhancement of SHC, while there is no enhancement of SHC for other solid–liquid mixtures with the particle in the microscale or even larger. The particle in the nanoscale has a much larger specific surface area than that of the microscale or millimeter-scale particle. There will be a much more compressed layer in the solid–liquid mixture system for the solid phase with a given quantitative. In order words, the nanoparticle can provide more constraint to the ions in the base salt than the bigger particle.

Based on the energy analysis and configuration analysis mentioned above, the second and third mechanisms mentioned in Section 1 (i.e., interfacial thermal resistance theory and compressed layer theory) should be the same thing, since they are both induced by the interaction between the nanoparticle and base salt. The interfacial thermal resistance and

the compressed layer only affect the appearance, rather than the mechanisms or the reason behind the SHC enhancement. In fact, the reason leading to the SHC enhancement of the molten salt-based nanofluid should be the force between nanoparticle and base salt. In other words, the constraint of the nanoparticle to the ion acts as the extra thermal storage device.

4. Conclusions

In the current work, we synthesized the molten salt-based nanofluid and measured the SHC of the nanofluid with nanoparticle loadings of 0.2, 0.6, 1.0, and 1.5% in mass fraction. The results show that the addition of the nanoparticle indeed enhanced the specific heat capacity of the base salt, and the enhancement ranged from about 1 to 21%. The thermal equilibrium model cannot be used to calculate the SHC of a molten salt-based nanofluid. Meanwhile, the microstructures were observed by SEM in this research. The SEM images showed that the SHC enhancement has a positive correlation with the nanoparticle dispersion. Better dispersion can provide larger SHC enhancements.

Furthermore, the mechanisms behind the SHC enhancement mentioned in the previous literature, which are generally accepted by the majority of researchers (i.e., higher nanoparticle SHC theory, interfacial thermal resistance theory, and compressed layer theory), were investigated by molecular dynamics simulations. The MD simulation results demonstrated that the nanoparticle SHC is higher than that of the bulk materials, however, still lower than that of the base salt. Hence, the higher nanoparticle SHC does not correlate with the SHC enhancement of the base salt. As for the two other theories, the results indicate that they both are caused by the extra force between the nanoparticle and the base salt, and the constraint of the nanoparticle to the ion acts as the extra thermal storage device (enhanced specific heat capacity).

Furthermore, some inference can also be obtained from our investigation. For instance, selecting a nanoparticle with the properties that can provide larger Van der Waals forces between the nanoparticle and base salt should provide a greater enhancement in the heat storage. Meanwhile, the nanoparticle with a stronger polarity and higher chemical valence maybe also more beneficial to the enhanced specific heat capacity, since they can provide a stronger Coulombic force. In other words, the results in this paper can provide guidance on the selection of the material and the thermophysical property prediction for the molten salt-based nanofluid, to a certain extent.

In the future, we will continue to investigate the force between the nanoparticle and the base salt, aiming at different nanoparticle and based fluids. Besides, the quantitative study would also be applied to the investigation of force analysis for different molten salt nanofluids. We believe that our research can be applied to a broader molten salt-based nanofluid and offers possible avenues for optimizing the nanoparticle by developing clusters that have functionalized surface layers to maximize the constraint with the fluid molecules.

Author Contributions: Formal analysis, B.L.; funding acquisition, X.D.; investigation, Z.L., L.C. and B.L.; methodology, Z.L.; project administration, B.L. and X.D.; software, Z.L. and L.C.; writing—original draft, Z.L.; writing—review and editing, Z.L. All authors have read and agreed to the published version of the manuscript.

Funding: This research received no external funding.

Institutional Review Board Statement: Not applicable.

Informed Consent Statement: Not applicable.

Data Availability Statement: Data is contained within the article, and the details can be available on request from the corresponding author.

Acknowledgments: This research was funded by the National Natural Science Foundation of China, grant number No. 51806064 and 51676069, and the Fundamental Research Funds for the Central Universities, grant number No. 2018QN034.

Conflicts of Interest: There are no conflicts of interest to declare.

References

1. Peiro, G.; Prieto, C.; Gasia, J.; Jove, A.; Miro, L.; Cabeza, L.F. Two-tank molten salts thermal energy storage system for solar power plants at pilot plant scale: Lessons learnt and recommendations for its design, start-up and operation. *Renew. Energy* **2018**, *121*, 236–248. [CrossRef]
2. Janz, G.J. *Molten Salts Handbook*; Elsevier: Amsterdam, The Netherlands, 1967.
3. González-Roubaud, E.; Pérez-Osorio, D.; Prieto, C. Review of commercial thermal energy storage in concentrated solar power plants: Steam vs. molten salts. *Renew. Sustain. Energy Rev.* **2017**, *80*, 133–148.
4. Chen, X.; Wu, Y.-t.; Wang, X.; Ma, C.-f. Experimental study on the specific heat and stability of molten salt nanofluids prepared by high-temperature melting. *Solar Energy Mater. Solar Cells* **2018**, *176*, 42–48. [CrossRef]
5. Anagnostopoulos, A.; Alexiadis, A.; Ding, Y. Molecular dynamics simulation of solar salt (NaNO3-KNO3) mixtures. *Solar Energy Mater. Solar Cells* **2019**, *200*, 109897. [CrossRef]
6. Mohan, G.; Venkataraman, M.B.; Coventry, J. Sensible energy storage options for concentrating solar power plants operating above 600 °C. *Renew. Sustain. Energy Rev.* **2019**, *107*, 319–337. [CrossRef]
7. Sohal, M.S.; Ebner, M.A.; Sabharwall, P.; Sharpe, P. *Engineering Database of Liquid Salt Thermophysical and Thermochemical Properties*; Idaho National Laboratory (INL): Idaho Falls, ID, USA, 2010.
8. Arthur, O.; Karim, M.A. An investigation into the thermophysical and rheological properties of nanofluids for solar thermal applications. *Renew. Sust. Energ. Rev.* **2016**, *55*, 739–755. [CrossRef]
9. Araki, N.; Matsuura, M.; Makino, A.; Hirata, T.; Kato, Y. Measurement of thermophysical properties of molten salts: Mixtures of alkaline carbonate salts. *Int. J. Thermophys.* **1988**, *9*, 1071–1080. [CrossRef]
10. Nunes, V.; Queirós, C.; Lourenço, M.; Santos, F.; De Castro, C.N. Molten salts as engineering fluids–A review: Part I. Molten alkali nitrates. *Appl. Energy* **2016**, *183*, 603–611.
11. Serrano-López, R.; Fradera, J.; Cuesta-López, S. Molten salts database for energy applications. *Chem. Eng. Process. Process. Intensif.* **2013**, *73*, 87–102. [CrossRef]
12. Wei, X.; Yin, Y.; Qin, B.; Wang, W.; Ding, J.; Lu, J. Preparation and enhanced thermal conductivity of molten salt nanofluids with nearly unaltered viscosity. *Renew. Energy* **2020**, *145*, 2435–2444. [CrossRef]
13. Sang, L.; Ai, W.; Wu, Y.; Ma, C. SiO_2-ternary carbonate nanofluids prepared by mechanical mixing at high temperature: Enhanced specific heat capacity and thermal conductivity. *Solar Energy Mater. Solar Cells* **2019**, *203*, 110193. [CrossRef]
14. Dudda, B.; Shin, D. Effect of nanoparticle dispersion on specific heat capacity of a binary nitrate salt eutectic for concentrated solar power applications. *Int. J. Therm. Sci.* **2013**, *69*, 37–42. [CrossRef]
15. Zhang, Q.; Wang, Z.; Du, X.; Yu, G.; Wu, H. Dynamic simulation of steam generation system in solar tower power plant. *Renew. Energy* **2019**, *135*, 866–876. [CrossRef]
16. Xiong, Y.; Sun, M.; Wu, Y.; Xu, P.; Xu, Q.; Li, C.; Ding, Y.; Ma, C. Effects of Synthesis Methods on Thermal Performance of Nitrate Salt Nanofluids for Concentrating Solar Power. *Energy Fuels* **2020**, *34*, 11606–11619. [CrossRef]
17. Seo, J.; Shin, D. Size effect of nanoparticle on specific heat in a ternary nitrate ($LiNO_3$ –$NaNO_3$–KNO_3) salt eutectic for thermal energy storage. *Appl. Therm. Eng.* **2016**, *102*, 144–148. [CrossRef]
18. Sang, L.; Liu, T. The enhanced specific heat capacity of ternary carbonates nanofluids with different nanoparticles. *Solar Energy Mater. Solar Cells* **2017**, *169*, 297–303. [CrossRef]
19. Luo, Y.; Du, X.; Awad, A.; Wen, D. Thermal energy storage enhancement of a binary molten salt via in-situ produced nanoparticles. *Int. J. Heat Mass Transf.* **2017**, *104*, 658–664.
20. Shin, D.; Banerjee, D. Enhancement of specific heat capacity of high-temperature silica-nanofluids synthesized in alkali chloride salt eutectics for solar thermal-energy storage applications. *Int. J. Heat Mass Transf.* **2011**, *54*, 1064–1070. [CrossRef]
21. Mondragon, R.; Julia, J.E.; Barba, A.; Jarque, J.C. Characterization of silica–Water nanofluids dispersed with an ultrasound probe: A study of their physical properties and stability. *Powder Technol.* **2012**, *224*, 138–146. [CrossRef]
22. Chen, Y.; Huang, Y.; Li, K. Temperature effect on the aggregation kinetics of CeO_2 nanoparticles in monovalent and divalent electrolytes. *J. Environ. Anal. Toxicol* **2012**, *2*, 158–162.
23. Andreu-Cabedo, P.; Mondragon, R.; Hernandez, L.; Martinez-Cuenca, R.; Cabedo, L.; Enrique Julia, J. Increment of specific heat capacity of solar salt with SiO_2 nanoparticles. *Nanoscale Res. Lett.* **2014**, *9*. [CrossRef] [PubMed]
24. Li, Z.; Li, B.; Du, X.; Wu, H. Experimental investigation on stability of thermal performances of solar salt based nanocomposite. *Renew. Energy* **2020**, *146*, 816–827. [CrossRef]
25. Hu, Y.; He, Y.; Zhang, Z.; Wen, D. Effect of Al_2O_3 nanoparticle dispersion on the specific heat capacity of a eutectic binary nitrate salt for solar power applications. *Energy Convers. Manag.* **2017**, *142*, 366–373. [CrossRef]
26. Hu, Y.; He, Y.; Zhang, Z.; Wen, D. Enhanced heat capacity of binary nitrate eutectic salt-silica nanofluid for solar energy storage. *Solar Energy Mater. Solar Cells* **2019**, *192*, 94–102. [CrossRef]
27. Testing ASF. *Materials. Standard Test Method for Determining Specific Heat Capacity by Differential Scanning Calorimetry*; ASTM International: West Conshohocken, PA, USA, 2011.
28. Palmer, M. Propagation of Uncertainty through Mathematical Operations. pp. 1–7. Available online: http://web.mit.edu/fluids-modules/www/exper_techniques/ (accessed on 29 January 2021).

29. Betts, M.R. The effects of nanoparticle augmentation of nitrate thermal storage materials for use in concentrating solar power applications. Master's Thesis, Texas A & M University, College Station, TX, USA, 2011.
30. Ho, M.X.; Pan, C. Optimal concentration of alumina nanoparticles in molten Hitec salt to maximize its specific heat capacity. *Int. J. Heat Mass Transf.* **2014**, *70*, 174–184. [CrossRef]
31. Li, Y.; Chen, X.; Wu, Y.; Lu, Y.; Zhi, R.; Wang, X.; Ma, C.J.S.E. Experimental study on the effect of SiO_2 nanoparticle dispersion on the thermophysical properties of binary nitrate molten salt. *Solar Energy* **2019**, *183*, 776–781. [CrossRef]
32. Qiao, G.; Lasfargues, M.; Alexiadis, A.; Ding, Y. Simulation and experimental study of the specific heat capacity of molten salt based nanofluids. *Appl. Therm. Eng.* **2017**, *111*, 1517–1522. [CrossRef]
33. Buongiorno, J. Convective transport in nanofluids. *J. Heat Transf.* **2006**, *128*, 240–250. [CrossRef]
34. Choi, S.U.; Eastman, J.A. *Enhancing Thermal Conductivity of Fluids with Nanoparticles*; Argonne National Laboratory: Lemont, IL, USA, 1995.
35. Wang, L.; Tan, Z.; Meng, S.; Liang, D.; Li, G. Enhancement of molar heat capacity of nanostructured Al2O3. *J. Nanopart. Res.* **2001**, *3*, 483–487.
36. Wang, B.-X.; Zhou, L.-P.; Peng, X.-F. Surface and Size Effects on the Specific Heat Capacity of Nanoparticles. *Int. J. Thermophys.* **2006**, *27*, 139–151. [CrossRef]
37. Cui, L.; Feng, Y.; Tang, J.; Tan, P.; Zhang, X. Heat conduction in coaxial nanocables of Au nanowire core and carbon nanotube shell: A molecular dynamics simulation. *Int. J. Therm. Sci.* **2016**, *99*, 64–70. [CrossRef]
38. Li, Z.; Cui, L.; Li, B.; Du, X. Enhanced heat conduction in molten salt containing nanoparticles: Insights from molecular dynamics. *Int. J. Heat Mass Transf.* **2020**, *153*, 119578. [CrossRef]
39. Nosé, S. A unified formulation of the constant temperature molecular dynamics methods. *J. Chem. Phys.* **1984**, *81*, 511–519. [CrossRef]
40. Hoover, W.G. Canonical dynamics: Equilibrium phase-space distributions. *Phys. Rev. A* **1985**, *31*, 1695.
41. Jund, P.; Jullien, R. The glass transition in a model silica glass: Evolution of the local structure. *Philos. Mag. A* **1999**, *79*, 223–236. [CrossRef]
42. Shi, D.; Guo, Z.; Bedford, N. 1—Basic Properties of Nanomaterials. *Nanomater. Devices* **2015**, 1–23. [CrossRef]
43. Qiao, G.; Alexiadis, A.; Ding, Y. Simulation study of anomalous thermal properties of molten nitrate salt. *Powder Technol.* **2017**, *314*, 660–664. [CrossRef]
44. Yuan, F.; Li, M.-J.; Qiu, Y.; Ma, Z.; Li, M.-J. Specific heat capacity improvement of molten salt for solar energy applications using charged single-walled carbon nanotubes. *Appl. Energy* **2019**, *250*, 1481–1490. [CrossRef]